DR RICHARD M LAINE (Orcid ID : 0000-0003-4939-3514)

Article type : Article

Corresponding Author mail id:-talsdad@umich.edu

Chemical Modification at and within Nanopowders: Synthesis of Core-shell Al_2O_3@TiON Nanopowders via Nitriding nano-$(TiO_2)_{0.43}(Al_2O_3)_{0.57}$ Powders in NH_3

F. You,[1,3] K. Sun,[1] E. Yi,[1] E. Nakatani,[2] N. Umehara[2] and R.M. Laine*[1]

[1]Department of Materials Science and Engineering, University of Michigan, Ann Arbor, MI 48109, USA

[2]Department of Mechanical Engineering, Nagoya University, Nagoya, Japan

[3]Institute of Fire Science and Engineering, Nanjing Tech University, Nanjing, Jiangsu 210009, China

Abstract

Here we demonstrate the potential utility of using chemical modification to reorganize metastable nanoparticles into nanostructured nanoparticles without coincidentally inducing extensive necking/sintering. The motivation for this effort derives from the concept that chemical reduction of a single component in a mixed-metal nanoparticle will create segregated islands of a second immiscible phase. Given the very high chemical energies inherent in nanoparticles, the formation of even smaller islands of a second

phase can be anticipated to lead to extremely high interfacial energies that may drive these islands to diffuse to cores or surfaces to form core-shell structures that minimize such interfacial energies. Thus, ammonolysis of $(TiO_2)_{0.43}(Al_2O_{3)0.57}$ composition nanopowders where both elements are approximately uniformly mixed at atomic length scales, under selected conditions (1000 °C) for various periods of time at constant NH_3 flow rates leads primarily to the reduction of the Ti species to form TiN or TiON which then appears to diffuse to the surface of the particles. The final products consist of Al_2O_3@TiON core-shell nanopowders that remain mostly unaggregated pointing to a new mechanism for modifying nanopowder chemistries and physical properties.

Key words: Mixed metal oxide nanopowders; nitridation; core-shell; phase separation; nanostructured nanopowders

Introduction

Nano science and engineering now consist of multiple separate fields of research driven by the promise that nanomaterials offer novel properties that can differ greatly from bulk materials of the same composition, or because they can offer significant processing benefits arising from the paradigm of "bottom up processing," among other unique attributes. Many of the special features offered by nanoparticles (NPs) derive from the fact that a large fraction of the material lies close to high-energy, highly curved surfaces. This material is often much more reactive than bulk materials of the same composition, leading for example to much lower melting points, higher rates of atomic and ionic diffusion at or near particle surfaces or along grain boundaries in nano- or fine grained structures.[1-6] The work reported here explores the potential to selectively chemically transform one component in a mixed-metal oxide NP to drive phase segregation to generate nanocomposite NPs. In this initial study we use NH_3 to reduce and nitride Ti ions in $(TiO_2)_{0.43}(Al_2O_3)_{0.57}$ NPs. The end products remain as NPs with some aggregation but offer core-shell structures with the shell consisting of TiON and the core Al_2O_3.

Our initial intent was not to produce core-shell materials but simply to demonstrate

the potential utility of selective chemical modification of a single metal oxide component in mixed-metal oxide NPs with the objective of developing a novel route to sets of nanocomposite NPs. However, core-shell materials have been found to offer a wide variety of properties not found in simple mixtures of the components as discussed in multiple articles.[7-13]

In our own work, for example, LF-FSP core-shell ZrO_2-Al_2O_3 powders were shown to sinter to fully dense composites at 1120° C with AGSs < 200 nm.[14,15] This contrasts with efforts to sinter mixtures of the same powders that required temperatures in excess of 1400°C. Likewise, core-shell [($Ce_{0.7}Zr_{0.3}O_2$)@Al_2O_3] NPs exhibited unprecedented catalytic properties arising from novel chemistries.[16] Most recently we also demonstrated that LF-FSP could be used to produce Pd@ZrO_2 core@shell catalysts that offer novel catalytic activities because of the protection of the metal particle from sintering.[17] Thus, there is considerable motivation to develop routes to new core shell materials in addition to our original goal.

Liquid feed flame spray pyrolysis (LF-FSP) can be used to generate a wide variety of metastable mixed-metal oxide NPs. In this process, alcohol solutions of metallo-organics (typically metal carboxylates) of the target composition(s) are aerosolized with excess O_2, ignited with methane/O_2 pilot torches and then combusted at 900-1500 °C in a ≈ 1.5 m long quartz or stainless steel chamber. The resulting cloud of ions is quenched at rates < 100 msec to temperatures below 400 °C forming NPs that are then captured by electrostatic precipitation at rates of 10-100 g/h. The average particle sizes, APSs, are typically 20-100 nm and the recovered NP agglomerates are normally easily dispersed using simple milling. The "as-shot" NPs are often kinetic (metastable) rather than thermodynamic products. The degree of mixing in these NPs is such that the average composition of the precursor solution is reproduced in the NPs at length scales ranging from 1-50 nm.

For example, we produce δ-Al_2O_3 rather than α-Al_2O_3 even though flame temperatures are sufficient to effect phase transformation.[18,19] We find phase pure spinel for $(MO)_x(Al_2O_3)_{1-x}$ for M = Ni, Co, Mg, Zn (x = 0.1-0.25), compositions not found in their phase diagrams.[20,21] We produce hexagonal $Y_3Al_5O_{12}$ rather than YAG[22] and amorphous mullite composition $2SiO_2 \cdot 3Al_2O_3$ NPs.[23]

In the core-shell ZrO_2 and $Ce_xZr_{1-x}O_2$ NPs the shells are δ-Al_2O_3 shells.[14,15] The

ZrO_2 core is tetragonal. Because self-diffusion of δ-Al_2O_3 >> α-Al_2O_3 or t-ZrO_2, we can make 99$^+$% dense t-ZrO_2 toughened α-Al_2O_3 (ZTA) at 1:1 mol ratios by *pressureless sintering* at 1120°C with average grain sizes (AGSs) ≈ 200 nm; well below typical ZTA processing temperatures and with finer grain sizes.

In contrast to the Al_2O_3-ZrO_2 NPs, LF-FSP processing of precursor compositions along the Al_2O_3-TiO_2 tie-line provides NPs where the length scale of mixing is somewhat greater than atomic mixing.[18,19] In these powders, substitution of Al into the TiO_2 lattice coincidentally introduces oxygen vacancies that drive formation of the rutile phase rather than the commonly observed anatase phase. In this initial report, our objective was to probe diffusion at and within these NPs by selectively nitriding the TiO_x component with some surprising results.

Given that Ti^{4+} is more readily reduced than Al^{3+} in flowing NH_3,[24,25] the motivation for the current work was to determine if it was possible to chemically reduce Ti^{4+} using NH to form TiON or more preferably TiN within single NPs.

The thought experiment driving the work here is the idea of making nanostructured NPs. Basically as reduction occurs, we can envision two possible processes occurring as illustrated in Figure **1**. In one scenario, the reduced phase forms and segregates to form a "chocolate chip" ensemble of very fine particles within a single NP. Alternately, one might envision all of these NPs assembling and phase segregating to form core-shell systems. Logically, the energy required to form very high energy interfaces in the chocolate chip scenario may be so high that it drives diffusion of any intermediate "chips" to the surface or interior to diminish the overall surface free energy but forming a core, or a shell. Thus, in this experiment we would expect to see core-shell structures, which we do, however in a related system we see pebble like Ni nanoparticles on the surface of an alumina core.[17]

Experimental section

Materials. Titanium isopropoxide [$Ti(OiPr)_4$ or Tyzor TE], Aluminum hydroxide, Ethylene glycol and Triethanolamine [$N(CH_2CH_2OH)_3$, 98%] were purchased from Fischer Scientific (Pittsburgh, PA), Chattem Chemical Co. (Chattam, TN), Sigma-Aldrich (Milwaukee, WI) and Sigma-Aldrich (Milwaukee, WI), respectively. Anhydrous ethanol, 200 proof, was purchased from Decon Labs (King of Prussia, PA). A nitrogen

tank was provided by Metro Welding Supply Co. (Detroit, MI) to supply Extra Dry Grade (88471) nitrogen for inert protection of preparing pre- cursors of titanatrane and alumatrane. A 16 lbs. ammonia tank was purchased from Welding Supply Co. (Detroit, MI) to provide steady ammonia (purity 99.995%) for nitridation of nano- metal oxides prepared via the LF-FSP process. All chemicals were used as received.

Precursor Preparation. Alumatrane [$N(CH_2CH_2O)_3Al$] and titanatrane [$N(CH_2CH_2O)_3Ti\text{-}OCH(CH_3)_2$] were used as the alumina (Al_2O_3) and titania (TiO_2) sources, respectively. By mixing measured amounts of the two precursor solutions for LF-FSP in appropriate amounts, 500 mL of solutions of each of the precursor composition with the specified molar ratio corresponding to a ceramic powder system of $(TiO_2)_x(Al_2O_3)_{1-x}$ (x = 0.43) can be made via LF-FSP as basis for further nitridation. In the process 1050 mL anhydrous ethanol (EtOH) was added with stirring at 20 °C to dilute the mixed precursor solutions to be 3 wt% ceramic yield as measured by TGA.

Alumatrane. Aluminum hydroxide [$Al(OH)_3$, 156 g, 2.0 mol] was reacted with triethanolamine [TEA, $N(CH_2CH_2OH)_3$, 400 ml, 3.0 mol] in ethylene glycol which was used as solvent. The solvent was heated at 200 °C in flask with stirring under N_2 flow for several hours until the solution became transparent and golden in color. Alumatrane has a density of 0.96 g/cm and a ceramic content of 28.0wt% Al_2O_3. An alumatrane/ethanol solution was prepared that contained 7.4 wt% Al_2O_3 as determined by TGA.

Titanatrane. Titanium isopropoxide {TTIP, $Ti[OCH(CH_3)_2]_4$ or $Ti(OiPr)_4$, 1150 ml, 3.80 mol} was reacted with triethanolamine [$N(CH_2CH_2OH)_3$, 1010 ml, 7.60 mol] at a molar ratio of 1 to 2, in a 4 L vessel (three-necked Schlenk flask) with stirring under N_2 flow for 8 h to distill isopropanol off. The as-purchased titanatrane isopropoxide containing 20 wt% free *i*PrOH has a density of 0.99 g/cm^3. Triethanolamine was added slowly with an addition funnel while the mixture was stirred constantly over a 4 h period. The resulting titanatrane, dissolved in byproduct isopropanol, had a ceramic yield (TiO_2) of 11.5 wt % confirmed by TGA.

Liquid-Feed Flame Spray Pyrolysis (LF-FSP). LF-FSP, as invented at the University of Michigan, has been described in detail in published papers.[5,6,14,15,17-23] The apparatus consists of a precursor- typically 3 wt% ceramic yield solution of precursor in an ethanol mixture is pumped (30-50 mL/min) to an ultrasonic atomizer with oxygen to generate an

oxygen-rich aerosol that is ignited via methane/oxygen pilot torches attached in the spray head (located in the ignition chamber).

Combustion occurs at ≥1 000 °C (1200-1500°C), producing Al_2O_3-TiO_2 NPs and gaseous byproducts, e.g. H_2O and CO_2. A steep temperature gradient (≥500 °C/s), between the combustion chamber and the 300 °C collection point (a temperature drop of 300-500 °C in a range of 1.5 m in ESP section) provides very rapid quenching (equivalent to a 1000 °C quench in ≤100 ms), as the kinetic powders are carried away from the combustion zone at a high velocity of 700 cfm using an inline radial pressure blower.

The powders are collected downstream by a radial pressure exhaust (19.8 m^3/min) in a pair of 2 m×8 cm. rod-in-tube ESP maintained at a 5-10 kV pseudo-dc potential. Due to the rapid quenching, particles formed are not aggregated but lightly agglomerated and break up easily on ultrasonication or ball-milling. The entire process is so rapid that atomically mixed nano-oxide particles form.

Typical powders are 15-100 nm APS with specific surface areas (SSAs) of 30-100 m^2/g. When combinations of elements are used, the resulting nanopowders will have compositions identical to those of the precursor solutions. Because compositions of chemical solutions can be changed intentionally, potentially even during mixing just before aerosolization, it becomes possible to combinatorially produce mixed-metal oxide materials. Hence it becomes possible to rapidly optimize materials for given properties or for ease of processing. After completion of a run, the powders were recovered from the ESP tubes and stored in plastic bags in air. No further effort was made to protect the powders from the atmosphere.

FBR design and operation. Al_2O_3-TiO_2 nanopowders (around 500 mg) prepared via LF-FSP were put into a quartz tube reactor and nitrided to 1000 °C for 1, 5, 10, 20, 30, 40 and 60 h in the flow of NH_3 gas using a tube furnace. A schematic of the quartz tube reactor for ammonolysis is shown in Figure **2**. Before introducing the NH_3 gas flow, the quartz tube reactor was first flushed with N_2 to eliminate air in the system. The sample was taken from the furnace after it had cooled to ≤100 °C. The gas flow rate and temperature ramping rate were 140 mL/min and 20 °C/min, respectively.

TGA-DTA. Phase transformations and mass loss events occurring during heating of as-prepared samples were investigated with a TGA-DTA (TA Instruments, Inc., New

Castle, DE). As-prepared nitrided powders of 15-30 mg were hand pressed in a 3 mm dual-action die, placed in- side alumina sample pans, and heated at ramp rates of 10 °C/min from ambient temperature to 1000 °C. A synthetic dry air low of 60 mL/min was maintained during all SDT experiments.

Scanning Transmission Electron Microscopy (STEM). A JEOL JEM-2100F (JOEL, Japan) aberration corrected STEM operated at 200kV with a SDD EDAX's energy dispersive spectroscopy (EDS) detector attached was used to study the microstructure and chemistry of the nanoparticles. TEM specimens were prepared by simply dusting some dry powders on holey carbon film coated Cu grids. STEM images were taken using both high-angle annular dark-field (HAADF) and bright-field detectors. Element mapping was performed using Ti, N, Al and O X-ray signals. To avoid carbon contamination in the mapping process, as-produced samples were exposed to low-power infrared for 10-20 min before tests.

X-Ray Photoelectron Spectroscopy (XPS). A Kratos Axis Ultra XPS (Kratos analytical, Manchester, U.K.) with a monochromated Al K_α (1.486 keV) source was used to analyze the chemistry of Ti, N, Al and O elements in nanopowders.

X-ray powder diffraction analyses (XRD). Both the as-produced and the nitrided samples were characterized using a Rigaku (Rigaku Denki., Ltd., Tokyo, Japan) Rotating Anode Goniometer XRD system (Cu Kα radiation (1.541 Å) with a Ni filter operating at 40 kV and 100 mA. The powder samples of around 100 mg were packed on a glass specimen holder (amorphous silica slides) for data collection.

Pellets were mounted to face the source on a metal sample holder. XRD scans were performed from 10° to 70° 2θ angles, using a scan rate of 2°/min and a 0.01° increments. Rietveld refinement and a 2-point linear background in the Jade program 2010 (Version 1.1.5 from Materials Data, Inc., Livermore CA) were used to determine the presence of any crystallographic phases and phase relations by comparing PDF files of standard materials. Peak position and intensities were characterized by comparison with ICDD files for γ-, δ-, δ*-, θ-, and α-alumina (00-050-0741, 00-046-1131, 00-046-1215, 00-023-1009, and 00-010-0173, respectively).[8] Peak positions and intensity for TiO, AlO and TiON were calculated using ICDD files, respectively. Vegard's law calculations were run using an internal Si(111) standard.

Scanning Electron Microscopy (SEM). The as-produced and the nitrided powders were studied by using a high-resolution SEM, a FEI NOVA Nanolab 200 FIB/SEM, (FEI company, Hillsboro, OR) in mode 2. An operating voltage of 15.0 kV was used. Powders were dropped onto conductive copper tape on a sample stub. Powder samples on the stubs were then sputter coated with gold/palladium (Au-Pd) for 2 min by using a Technics Hummer IV DC sputtering system (Anatech, Ltd., Alexandria, VA).

Diffuse Reflectance Fourier Transform (DRIFT) Spectra. Transmission and Diffuse reflectance Fourier transform (DRIFT) spectra were recorded on a Nicolet 6700 Series FTIR spectrometer (Thermo Fisher Scientific, Inc., Madison, WI). 400 mg of optical grade, random cuttings of KBr (International Crystal Laboratories, Garfield, NJ) were ground with an alumina pestle rigorously with 5 mg of the sample in an alumina mortar to be analyzed. The FTIR sample chamber was flushed continuously with N_2 for 10 min prior to data acquisition for an average of 100 scans in the range 4000-400 cm^{-1} with a precision of ± 4 cm^{-1}. New blank KBr reference samples were run every five samples. All data are reported in Kubelka-Munk units, so that intensity values are nearly linear with concentration.

Specific surface area (SSA) measurements. Specific surface areas of as-produced and nitride powders were obtained using a Micromeritics ASAP 2020 sorption analyzer (Micromerit-ics Inc., Norcross, GA). Powder samples (400 mg) were degassed at 200 °C under vacuum for 5- 8 h. Each analysis was run at -196 °C (77 K) with liquid N_2. The SSAs were determined by the BET multipoint method using ten data points at relative pressures of 0.05-0.30 p/po. SSAs were determined using the Brunauer-Emmett-Teller (BET) method and APSs (<R>) were calculated using the formula $R = 6/[\rho(SSA)]$ where R is the diameter of the average particle (APS) and ρ is the theoretical density of the material in g/cm^3. The densities of the powders were calculated using the rule of mixtures, which is an accepted method of obtaining the values for the properties of well-behaved composite materials, such as these intimately mixed nanopowders. The rule of mixtures is a weighted average using the volumetric fraction of the phases present rather than the mass fraction. Rule of Mixtures: $P = P\ \nu + P\ \nu$, where P is a property and ν is volume fraction. Analysis was done with the software package supplied with the instrument.

Results and discussion

As noted above, the high energy surfaces coupled with the metastable nature of our NPs offer a unique opportunity to probe diffusion in NPs without also causing sintering (necking) and may lead to novel ways to modify these materials for a variety of applications (e.g. making novel composites, catalysts, etc). Thus, transition metal, silica and boron based compounds are relatively easy to nitride/reduce using NH_3 at temperatures ca. 1000 °C.[24-32] In contrast, alumina nitrides easily only above 1100 °C.[33,34] A variety of metal oxides when treated in flowing NH_3, from oxynitrides, nitrides and metal.[35] Transition metals are most easily reduced and/or nitrided.[36,37] In previous studies, we used a fluidized bed approach to nitriding; transforming SiO_2 and cordierite to their oxynitrides.[24,38]

Traditionally fluidized bed reactors (FBRs) fully suspend particles in a gas flow. With NPs, any strong gas flow entrains particles and despite using fine filters, the NPs either rapidly depart the FBR or clog filters. Thus, our efforts to nitride NPs use minimal gas flows that still cause the NPs to continually reorient in the FBR chamber but limit entrainment.[24] The current studies were partially motivated by the fact that the introduction of N or C to the titania lattice reduces its band gap providing materials that more readily absorb visible light and offer potential as photo catalysts. Given that heterogeneous catalyst activity is often directly proportional to surface area, the generation of TiO_xN_{1-x} species on a high surface area alumina support might be anticipated to offer improved catalytic properties. Thus, we hypothesized that nitriding our previously synthesized $(TiO_2)_{0.43}(Al_2O_3)_{0.57}$ NPs might provide new higher active photocatalysts. A further potential application would be to use these NPs to process fine-grained TiN/α-Al_2O_3 composites for structural/electrode applications, like the t-ZrO_2@Al_2O_3 NPs noted above.[15,39]

<u>Characterization of $(TiO_2)_{0.43}(Al_2O_3)_{0.57}$</u>.

Figure **3** presents the whole pattern fitting of the XRD of the as-shot powder. A more detailed analysis is presented in Figure **S1**. The data are similar to that published previously for $(TiO_2)_{0.5}(Al_2O_3)_{0.5}$.[19] The previous Rietveld compositional analysis suggests that these NPs consist of 76 wt % of θ and η-Al_2O_3 with rutile accounting for ca. 17 % of the material whereas the current material consists of 69 wt. % alumina and 28 wt % rutile.

The alumina phase was previously found to contain up to 15 at % Ti^{4+}.[19] We assume that the current alumina phase also contains some Ti^{4+} and likewise accounts for the "missing" Ti that is not reflected by the apparent analytical composition. Likewise, we find that the rutile phase also probably has some Al^{3+} sitting on Ti^{4+} sites favoring formation of the rutile phase based on regular oxygen vacancies that must exist so that there is charge balance, as we have discussed previously.[19]

The FTIR of this material (not shown) is also similar to that previously published[19] suggesting intimate mixing of both components, agreeing with element mapping studies described below.

Figure **4** provides secondary electron SEM images taken from the (a) as-shot $(TiO_2)_{0.43}(Al_2O_3)_{0.57}$ and (b)60 h-nitrided NPs. It shows that the as-shot powders consist of a bimodal distribution of spherical particles with some having ≈100 nm ave. diameters and the other ≈ 10 nm. The larger particles are likely simply agglomerates of the smaller particles because after 60 h nitriding, the big spherical particles have almost all disappeared. All the 60 h particles show irregular shapes with smaller sizes distribution.

Figure **5** shows TEM bright-field (BF) images of the as-shot (a) and 60 h-nitrided (b) $(TiO_2)_{0.43}(Al_2O_3)_{0.57}$. The morphologies of the particles in the two samples are similar to what can be seen from the SEM images but with more detailed features seen due to the higher spatial resolution for TEM imaging. The particles in the as-shot sample have spherical shapes with different sizes. In contrast, the particles in the 60 h nitrided sample have irregular shaped particles with more homogeneous size distribution. Some of the particles seem to have hollow interiors like those indicated by red arrows in (b) suggesting core-shell structures formed.

Figure **6** displays high-resolution electron microscopy (HREM) images taken from the as-shot and the 60 h nitrided samples. These images confirm that the crystal states of the particles in the two samples. The HREM image in (b) shows a particle with a possible core-shell structure based on the contrast difference between the center and the edge. To disclose the crystal structure of the core and the shell, two regions are outlined with their FFT displayed in (c) and (d), respectively. The two patterns can be indexed by the δ-AlO_x and TiN_xO_{1-x} phases.

To further confirm the core-shell nature of such particles, element mapping was per-

formed together with high angle annular dark-field (HAADF) imaging on the 60 h nitrided powders (Figure. **7**). The mapping data indicate that the core of the outlined particle has only Al and O with the shell having mainly Ti, N and O possibly some Al, consistent with the contrast in the HAADF image. The core has darker contrast as it has lighter elements (Al and O) and the shell shows brighter as it has relatively heavier element (Ti).

In comparison, element mapping was also performed on the powders in the as-shot sample shown in Figure **8**. The data show that the Al, Ti, N and O elements distributed uniformly in the powders.

Element mapping when combined with XRD and FTIR data for $(TiO_2)_{0.43}(Al_2O_3)_{0.57}$ composition powders suggests that the length scale of mixing is sub-10 nm in accord with the previous Rietveld refinement data and the current whole pattern mapping of Figure **3** that shows APSs are 5-8 nm for the major phases. This material and commercial TiO_2 (as-shot results very similar) were nitrided providing the data summarized in Table **1**.

It is possible to estimate the degree of nitridation using the mass gains in the Figure **9** TGAs (Table **1**). Pure TiN on oxidation to pure TiO_2 should exhibit a mass gain of 29 wt %. Pure LF- FSP TiO_2 and commercial TiO_2 were nitrided in flowing NH_3 using standard conditions at various temperatures. LF-FSP TiO_2 was nitrided under conditions targeting limited loss of specific surface area (SSA); thus, at 750 °C/18 h, the BET SSAs went from 90 to 70 m /g.

The mass gain in the TGA was 18 wt % indicating incomplete reduction likely to an intermediate TiON phase, see XRD and XPS studies below. A commercial TiO_2 was nitrided at 850 °/6 h and 1000 °C/3 h leading to materials with mass gains of 21 and 24 wt % respectively coincident with SSAs unchanged at 850 °C but reduced from 52 m^2/g to 29 m^2/g at 1000 °C (see also ref. 26). Thus, there is a tradeoff in rate of nitridation with loss of SSA = aggregation/partial sintering. The incomplete nitridation can be interpreted as a combination of processes.

The rate of N introduction should asymptote as the rate of O displacement falls off with: (1) increasing N content, (2) loss of surface area; and (3) reduction in diffusion rates for both O and N in the now denser material. Thus, one might anticipate never producing pure TiN. Indeed, it might also be anticipated that TiON is more stable than TiN

under these conditions.[39,40] With these baseline results in hand, we can now examine nitridation processes in $(TiO_2)_{0.43}(Al_2O_3)_{0.57}$ as revealed in mass gains in Figure **9**, as recorded in Table **1**. Figure **S2** provides a more detailed image of the oxidation processes shown in Figure **9**.

The TGAs reveal mass gains at≈ 500 °C for nitridation times ≤ 20 h and thereafter a second oxidative mass gain at≈ 800 °C. TiN oxidizes to TiO_2 at ≈ 480 °C (not shown), Table **1** in keeping with the literature.[39,40] If all the TiO_2 in the $(TiO_2)_{0.43}(Al_2O_3)_{0.57}$ NPs was reduced to TiN, then theory indicates the mass gain would be 9 wt %. However, we see that the mass gains at≈ 500 °C level off at ≈ 6 wt %. These results suggest that the resulting product likely consists primarily of TiN with≈ 30 % TiON (same XRD powder pattern as TiN). Logic dictates that the second mass gain must be oxidation of some form of AlON or some TiAlON phase.[39] Oxidation of AlON powder (nominal composition $Al_{23}O_{27}N_5$) is reported to initiate at 900°C with a mass gain of≈ 3 wt %. [341] oxidation for "pure" AlON occurs most readily at 1100 °C.[41]

If this material were solely TiN, then all oxidation would occur at 480 °C and nothing should happen at 800 °C. If it were pure AlON, then oxidation should not initiate until 900 °C rather than >760 °C. Thus, we believe that the Al in the matrix does nitride eventually giving a TiAlON phase rather than AlON, but only after TiON forms. m inor ox i-dation mass gain. Another possible perspective is that this slight oxidation occurs at the interface between TiON and Al_2O_3 in these core-shell systems that develop as seen below.[39,41]

Figures **5b** and **6b** and **7** suggest an unexpected transformation. Nitridation appears to "extract" Ti from the homogeneous $(TiO_2)_{0.43}(Al_2O_3)_{0.57}$ NPs to produce core-shell NPs where a shell of TiON (possibly with some Al) forms around a core of Al_2O_3. Examples of "donut" particles are seen in Figure **10**. Note that the TiO, TiON and TiN unit cell dimensions are very similar and as such it is not possible to discern a difference from XRD data, see Figures **S2** and **S3**. *The bottom line is NPs remain but with completely different morphologies*. Note that previous reports indicate that nitridation of TiO_2 can lead to formation of TiON hollow particles in support of the current observations.[26b]

Figure **7** analyses are in keeping with the global analyses determined by XPS. Figures **S4-S7** show the individual XPS spectra for Ti, Al and O of as-shot oxide and 60 h nitride

powders. As can be seen from Figure **S4**, after nitridation the Ti 2p shows noticeable variations in binding energy (differences for Ti 2p 3/2 and Ti 2p 1/2 are 2.3824 and 1.6666 eV) when compared to all other elements like Al and O, meaning the chemical surroundings change. When tracing the peak positions based on the NIST XPS database, other TiN_x, TiN_xO_y and Al_xO_y compositions are possible but no evidence is found for Al_xN_y, Al_xTi_y, $Al_xTi_yO_z$. A typical chemical formula found is $TiO_{0.37}N_{0.63}$ in keeping with the TGA results above.

To sum up, both osbornite TiO_xN_{1-x} and γ-Al_2O_3 (called transition alumina here) exist in the nanosized nitride powders with distinct grain boundaries, with a core-shell morphology.

Figure 10 shows the generally accepted mechanism for nitridation. The process initiates as NH bonds to metal Lewis acid sites. N-H cleavage follows with formation of M-N and O-H bonds then forming additional M-N bonds and releasing water vapor, which drives the reaction. Subsurface exchange depends on temperature and surface area as surface saturation drives substitution at greater depths.

In NPs where most material is near the surface, one might expect complete nitridation (Table **1** initial entries) or reduction to metals. However, one restraint is that introduced N causes densification, raises inherent viscosity and thereby reduces diffusion rates perhaps to the point where full nitridation is not possible. This is likely the reason TiAlON forms rather than TiN, which forms only at temperatures where considerable surface area is lost. The potential to completely nitride some materials is supported by the relative ease of nitriding thin films and fibers,[29-34] and much more difficult with large particles.[19] Rates of nitriding/reduction are surface area, temperature, flow rate, viscosity and material specific.

Conclusions

Based on the thought experiment presented in the introduction, we anticipated that reduction would preferentially lead to formation of core-shell nanopowders driven by the likelihood that the production of chocolate chip nanostructured nanopowders would create such high energy surfaces that the chips would like be driven to the core or to the surface as is seen. We presume this concept holds in the current study. A further important

observation is that it indeed possible to chemically modify metastable oxide nanopowders to reorganize into nanostructured nanopowders.

(1) A typical core-shell microstructure in nanosized as-produced nitride can be formed in as-produced nitride based on the starting oxide powders prepared via LF-FSP process in one- step. It is driven by the likelihood that the production of chocolate chip nanostructured nanopowders would create such high-energy surfaces that the chips would like be driven to the core or to the surface as is seen.

(2) Multiple crystalline phases are found in the as shot powder including rutile TiO_2, θ-alumina and Hongquiite TiO, and multiple crystalline phases of Osbornite $Ti_{0.88}O_{0.88}$, TiN, $TiN_{0.31}O_{0.31}$ and t-Al_2O_3 in as-produced nitride powders.

(3) A further important observation is that it indeed possible to chemically modify metastable oxide nanopowders to reorganize into nanostructured nanopowders.

Acknowledgements.

This work is supported by NSFC (51376089). JEOL JEM-2100F and the JEOL JEM-3100R05 aberration-corrected TEMs were under the support of the University of Michigan Col- lege of Engineering and NSF grant #DMR-0723032. The Kratos XPS was under the support of the University of Michigan College of Engineering and NSF grant #DMR-0420785. Thanks to Dr. Wei Liu for help in performing some STEM and HRTEM imaging.

References

1. J. Pan, "Solid-state diffusion under a large driving force and the sintering of nanosized particles," *Philos. Mag. Lett*. **84**, *303–310* (2004).
2. H. Gleiter, "Nanostructured materials: basic concepts and microstructure," *Acta Mater*. 48, 1-29 (2000).
3. R. W. Siegel, "Nanostructured materials," in Mechanical Properties and Deformation Behavior of Materials Having Ultra-Fine Microstructures (Proc. NATO Advanced Study Institute, Verneiro, 1992), M. Nastasi D. M. Parkin, H. Gleiter, eds. (Kluwer

Acad. Publ., Dordrecht, 1993) *p. 3-36*.

4. R. W. Siegel, "Nanostructured materials-mind over matter", *Nanostruct. Mater*. **3**, *1-18* (1993).
5. N. J. Taylor, R. M. Laine, "Bottom up processing is not always optimal. YAG tubes," *Adv. Functional Mater*. **24**, 1125-1132 (2014).
6. E. Yi, W. Wang, J. Kieffer, and R. M. Laine,"Flame made nanoparticles permit processing of dense, flexible, Li+ conducting ceramic electrolyte thin films of cubic-$Li_7La_3Zr_2O_{12}$ (c- LLZO)," *J. Mater. Chem. A* **4**, 12947–12954 (2016).
7. J. Lai, K. V. P. M. Shafi, A. Ulman, K. Loos, R. Lee, Y. Popovitz-Biro, T. Vogt, C. Estournes, "One-Step Synthesis of Core(Cr)/Shell(-Fe_2O_3) Nanoparticles," J. Am. Chem. Soc**. 127** 5730-5731 (2005).
8. S. Kim, B. Fisher, H.-J. Eisler, M. Bawendi, "Type-II Quantum Dots: CdTe/CdSe (Core/Shell) and CdSe/ZnTe (Core/Shell) Heterostructures," J. Am. Chem. Soc. **125** 11466-1146 (2003).
9. O. Masala, R. Seshadri, "Spinel Ferrite/MnO Core/Shell Nanoparticles: Chemical Synthesis of All-Oxide Exchange Biased Architectures," J. Am. Chem. Soc. **127** 9354-9355 (2005).
10. H. Sakai, T. Kanda, H. Shibata, T. Ohkubo, M. Abe, "Preparation of Highly Dispersed Core/Shell-type Titania Nanocapsules Containing a Single Ag Nanoparticle," J. Am. Chem. Soc; **128** 4944-4945 (2006).
11. K. Aslan, M. Wu, J. R. Lakowicz, C. D. Geddes, "Fluorescent Core-Shell Ag@SiO_2 Nanocomposites for Metal-Enhanced Fluorescence and Single Nanoparticle Sensing Platforms," J. Am. Chem. Soc; **129** 1524-1525 (2007).
12. C-C. Chung, J-H. Jean, "Aqueous Synthesis of Y_2O_2S:Eu/Silica Core-Shell Particles, "J. Am. Ceram. Soc. **88**, 1341-1344 (2005).
13. T-Y. Chen, P. Somasundaran," Preparation of Novel Core-Shell Nanocomposite Particles by Controlled Polymer Bridging," J. Am. Ceram. Soc. **81**, 140-144 (1998).
14. M. Kim, R. M. Laine, "A one-step synthesis of core-shell $(Ce_{0.7}Zr_{0.3}O_2)_x(Al_2O_3)_{1-x}$ [$(Ce_{0.7}Zr_{0.3}O_2)$@Al_2O_3] nanopowders via liquid-feed flame spray pyrolysis (LF-FSP)," J. Am. Chem. Soc. **131**, 9220-9 (2009).
15. Kim, M.; Laine, R. M.; "Pressureless sintering t-zirconia@δ-Al_2O_3 (54 mole%) core-

shell nanopowders at 1120°C for dense t-zirconia toughened δ-Al_2O_3 nanocomposites," *J. Am. Ceram. Soc.* **93**, 709-715 (2010).

16. B. Weidenhof, M. Reiser, K. Stöwe, W. F. Maier, M. Kim, J. Azurdia, E. Gulari, E. Sekkers, A. Barks, and R. M. Laine, "High Throughput Screening of Nanoparticle Catalysts Made by Flame Spray Pyrolysis as Hydrocarbon/NO Oxidation Catalysts; Active, Pt free catalysts," *J. Am. Chem. Soc*. **131**, 9207-19 (2009).
17. a. C. Y. Seo, E. Yi, X. Chen, R. M. Laine, G. B. Fisher, J. W. Schwank, "Single-step synthesis of Pd@ZrO_2 core@shell catalysts via colloid-feed flame spray pyrolysis, *Mater. Lett.* **206**, 105–108 (2017). b. H. Shirae, K. Hasegawa, H. Sugime, E. Yi, R. M. Laine, S. Noda, "Catalyst Nucleation and Carbon Nanotube Growth from Flame-Synthesized Co-Al-O Nanopowders at Ten- Second Time Scale," *Carbon*, **114**, 31-38 (2017).
18. T. Hinklin, B. Toury, C. Gervais, F. Babonneau, J. J. Gislason, R. W. Morton, R. M. Laine, "Liquid-Feed Flame Spray Pyrolytic Synthesis of Nanoalumina Powders," *Chem. Mater*. **16**, 21-30 (2004).
19. S. Kim, J. J. Gislason, R. W. Morton, X. Pan, H. Sun, R. M. Laine, "Liquid-Feed Flame Spray Pyrolysis of Nanopowders in the Alumina-Titania System, *Chem. Mater*. **16**, 2336-43 (2004).
20. R. M. Laine, T. R. Hinklin, J. Azurdia, M. Kim, J. C. Marchal, S. Kumar, "Finding Spinel in All the Wrong Places," *Adv. Mater*. **20**, 1373-75 (2008).
21. T. R. Hinklin, R. M. Laine, "Synthesis of metastable phases in the Magnesium Spinel- Alumina System," *Chem. Mater*. **20**, 553-558 (2008).
22. R. M. Laine, J. Marchal, H. J. Sun, X. Q. Pan, "A new $Y_3Al_5O_{12}$ phase produced by liq- uid-feed flame spray pyrolysis (LF-FSP)," *Adv. Mater*. **17**, 830-33 (2005).
23. R. Baranwal, M. P. Villar, R. Garcia, and R. M. Laine, "Synthesis, Characterization, and Sintering Behavior of Nano-mullite Powder and Powder Compacts," *J. Am. Ceram. Soc*. **84**, 951- 61 (2001).
24. C. R. Bickmore, R. M. Laine, "Processing Oxynitride Powders via Fluidized bed Ammonolysis of Large, Porous, Silica Paticles." *J. Am. Ceram. Soc*. **79**, 2865-77 (1996).
25. a. L. Zhang, Z. Lin, Y. Jiang, J. He, W. Cai, S. Li, "Synthesis of β-SiAlON

Nanopowder by Ammonolysis of Alumina–Silica Gel," *J. Am. Ceram. Soc*., **97**, 40–43 (2014). b. J. Sjoberg, and R. Pompe, "Nitridation of Amorphous Silica with Ammonia," *J. Am. Ceram. Soc*. **75**, 2189-2193 (1992).

26. a. H. Chen, A. Nambu, W. Wen, J. Graciani, Z. Zhong, J. C. Hanson, E. Fujita, J. A. Rodriguez, "Reaction of NH_3 with Titania: N-Doping of the Oxide and TiN Formation," *J. Phys. Chem. C* **111**, 1366-1372 (2007). b. J. H. Han, J. H. Bang, "A hollow titanium oxynitride nanorod array as an electrode substrate prepared by the hot ammonia induced Kirkendall effect," *J. Mater. Chem. A*, **2**, 10568-76 (2014).
27. H. O. Mulfinger, "Physical and Chemical Solubility of Nitrogen in Glass Melts," *J. Am. Ceram. Soc*. **49**, 462-67 (1966).
28. C. J. Brinker, "Formation of Oxynitride Glasses by Ammonolysis of Gels," *J. Am. Ceram. Soc*. **65**, C4-C5 (1982).
29. C. J. Brinker, D. M. Haaland, "Oxynitride Glass formation from Gels," *J. Am. Ceram. Soc*. **66**, 758-65 (1983).
30. P. Fink, B. Müller, G. Rudakoff, "Ammoniation and Nitridation of Highly Disperse Silica," *J. Non-Cryst. Solids*, **145**, 99-104 (1992).
31. R. Wusirika, "Reactions of Ammonia with Fumed Silica," *J. Am. Ceram. Soc*. **73**, 2926-29 (1990).
32. K. Kamiya, M. Ohya, T. Yoko, "Nitrogen-Containing SiO Glass Fibers Prepared by Ammonolysis of Gels Made from Silicon Alkoxides", *J. Noncryst. Sol*., **83**, 208-213 (1986).
33. J. Sappei, D. Goeuriot, F. Thevenot, P. L'Haridon, J. Guyader, Y. Laurent, "Nitridation of δ-alumina with ammonia," *Ceram. Int*. **17**, 137-42 (1991).
34. Q. Zhang, L. Gao, "Synthesis of Nanocrystalline Aluminum Nitride by Nitridation of δ- Al_2O_3 Nanoparticles in Flowing Ammonia," *J. Am. Ceram. Soc*. **89**, 415-421 (2006).
35. R. Marchand, Y. Laurent, J. Guyader, P. L'Haridon, P. Verdier, "Nitrides and Oxynitrides:Preparation, Crystal Chemistry and Properties," *J. Eur. Ceram. Soc*. **8**, 197-213 (1991).
36. C. Giordano, T. Corbiere, "A step forward in metal nitride and carbide synthesis: from pure nanopowders to nanocomposites," *Colloid. Polym. Sci*. **291**, 1297-1311

(2013).

37. Y M. Yang, M. J. MacLeod, F. Tessier, F. J. DiSalvo, "Mesoporous Metal Nitride Materials Prepared from Bulk Oxides," *J. Am. Ceram. Soc*. **95**, 3084-30 (2012).
38. R.M. Laine, C.R. Bickmore, K. F. Waldner, B. L. Mueller, H. W. Estry, "MgSiAlONs Prepared By Nitriding Cordierite Precursor Polymers with NH_3," in "Synthesis and Processing of Silicon Nitride Ceramics," Mat. Res. Soc. Symp. K Proc.; I-W. Chen, P.F. Becher, M. Mitomo, G. Petzow, T-S. Yen eds, *Mater. Res. Soc. Symp. Proc*. **287**, 251-256 (1993).
39. Y. G. Gogotsi, F. Porz, G. Dransfield, "Oxidation Behavior of Monolithic TiN and TiN Dispersed in Ceramic Matrices," *Oxidation of Metals*, **39**, 69-91 (1993).
40. H. Ichimura, A. Kawana, "High-temperature oxidation of ion-plated TiN and TiAIN films," *J. Mater. Res.* **8**, 1093-1100 (1993).
41. J. Q. Qi, M. X. Xie, Y. Wang, J. Wang, L. Xiao, N. Wei, D. Wu, T. C. Lu, "Non-isothermal and isothermal oxidation behaviors of AlON translucent ceramic in air," *Materials and Corrosion* **66**, 328-333 (2015).

Figure Captions

Figure 1. Possible modes of phase separation in metastable systems.

Figure 2. Schematic of the quartz tube reactor for ammonolysis.

Figure 3. Whole pattern fitting refinement of $(TiO_2)_{0.43}(Al_2O_3)_{0.57}$: 28 % rutile, 69 % t-alumina. (See the comment after mapping data).

Figure 4a. SEM images of as-shot and **b.** 60 h-nitrided $(TiO_2)_{0.43}(Al_2O_3)_{0.57}$ NPs.

Figure 5. TEMs of the as-shot (a) and (b) 60 h-nitrided $(TiO_2)_{0.43}(Al_2O_3)_{0.57}$ NPs.

Figure 6. HREM images of as-shot powders (a) and the 60h nitrided powders (b); (c) and (d) are FFT patterns from areas A and B in (b), respectively —latter is pure TiN_xO_{1-x}.

Figure 7. (a) HAADF image and (b) Ti, (c) N, (d) Al and (e) O maps taken from the 60 h nitride NPs, with one NP showing typical core-shell structure outlined.

Figure 8. (a) HAADF image and Ti (b), Al (c), and O (d) maps, respectively, from as-shot $(TiO_2)_{0.43}(Al_2O_3)_{0.57}$ NPs.

Figure 9. TGAs of $(TiO_2)_{0.43}(Al_2O_3)_{0.57}$ NPs FBR nitrided in NH_3/120 mL/min/1000°C for selected times.

Figure 10. Nitridation at an oxide surface as suggested by Mulfinger and others.[27-34]

Table Captions

Table 1. Nitridation vs time and temperature for TiO_2 and $(TiO_2)_{0.43}(Al_2O_3)_{0.57}$ NPs and oxidation mass gains after nitridation.

Sample	Process	XRD - WPF refinement wt %	SSA m^2/g	*mass gain wt %	Fully nitrided mass gain theory

					(wt %)
TiO_2	As-shot	A (82) R (18)	90	- 1.9	-
	750℃/18h /NH_3	TiN (90) A (7) R (3)	68	18	29 ($TiN \rightarrow TiO_2$)
TiO_2 (Commercial)	As-received	A (85) R (15)	52	- 1.8	-
	850℃/6h/ NH_3	TiN (100)	51	21	29 $TiN \rightarrow TiO_2$
	1000℃/3h /NH_3	TiN (100)	29	24	
$(TiO_2)_{0.43}(Al_2O_3)_{0.57}$	As-shot	T (94), R (6)	63	- 2.2	-
	750℃/18h /NH_3	T (96) TiN (4)	66	3	9 $0.43TiN \rightarrow 0.43TiO_2$
	950℃/15h /NH_3	T (86) TiN (14)	56	5.5	
$(TiO_2)_{0.43}(Al_2O_3)_{0.57}$ NH_3/1000℃ /h (SSA, m^2/g)	Mass loss Temp. ℃ (%)	1st Mass gain Temp. ℃ (%)	$(TiON)_x(TiO_2)_{0.43-x}$ x =	2nd Mass gain Temp. ℃ (%)	$(AlO_z)_{0.57-y}(TiAlON)_y$ theory mass gain 7.8 %
1 (58)	194 (1.7)	530 (4.6)		--	y = 0
5 (55)	226 (1.8)	560 (5.4)	x ≈ 0.22	--	y ≈ 0
10 (59)	238 (1.5)	568 (5.8)	x ≈ 0.22	--	y ≈ 0
20 (55)	246 (2.0)	570 (6.0)	x ≈ 0.22	--	y ≈ 0
30 (59)	292 (2.2)	615 (6.3)	x ≈ 0.22	780 (0.1)	y ≈ 0.5
40 (52)	270 (2.4)	615 (6.5)	x ≈ 0.22	760 (~0)	y ≈ 0.5
60 (5)	270 (2.2)	620 (6.0)	x ≈ 0.22	790 (0.5)	y ≈ 0.5

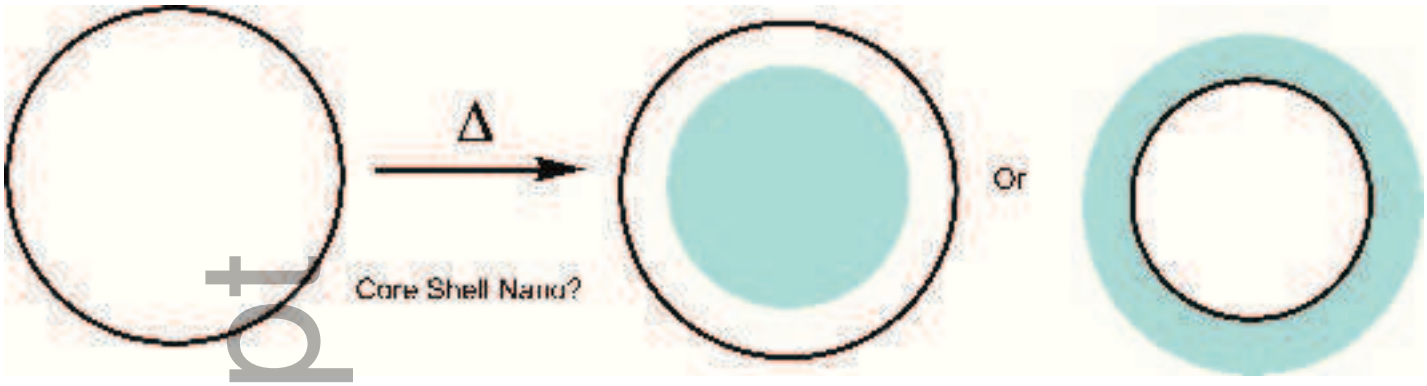

jace_15303_f1.tiff

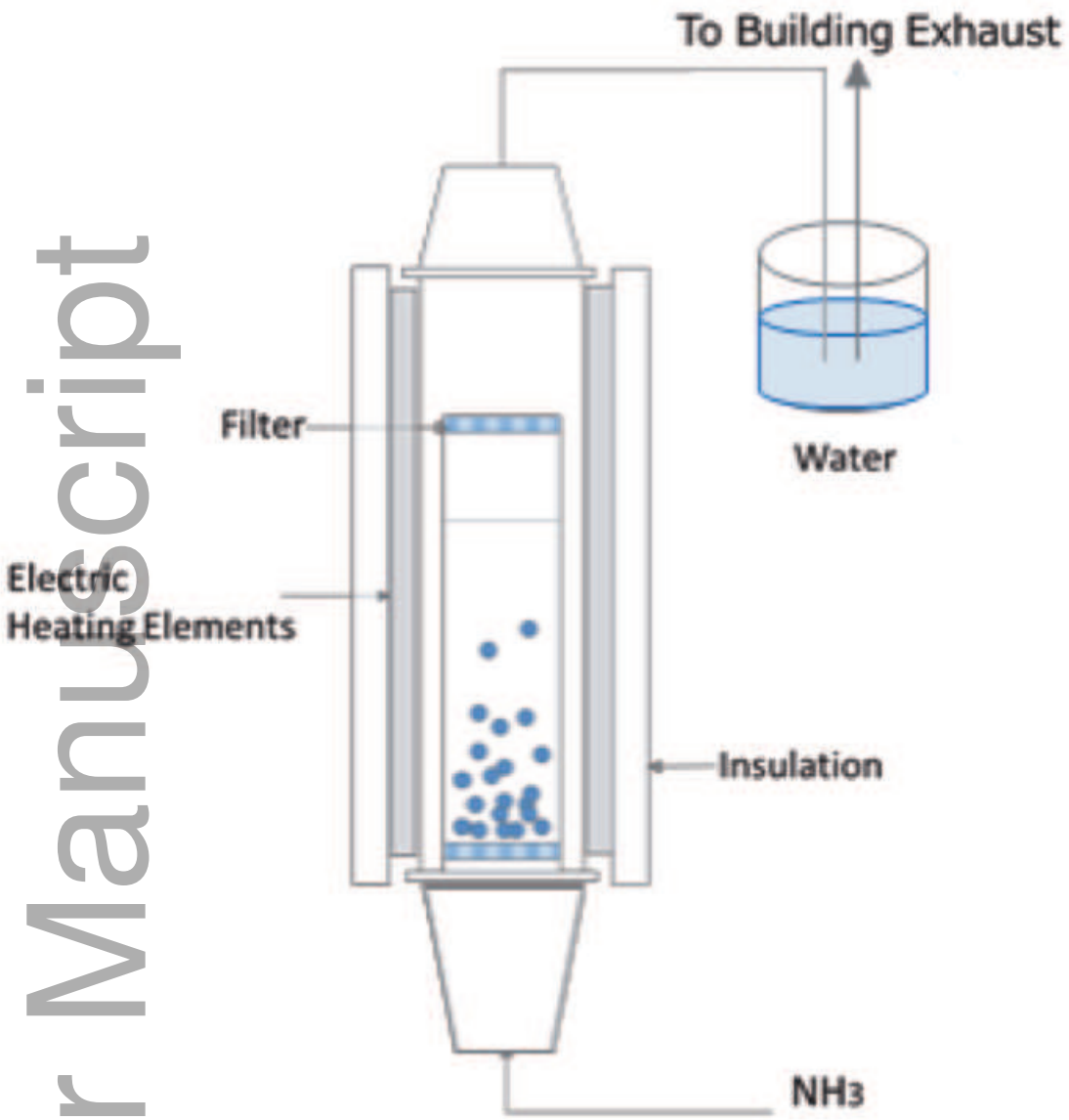

jace_15303_f2.tiff

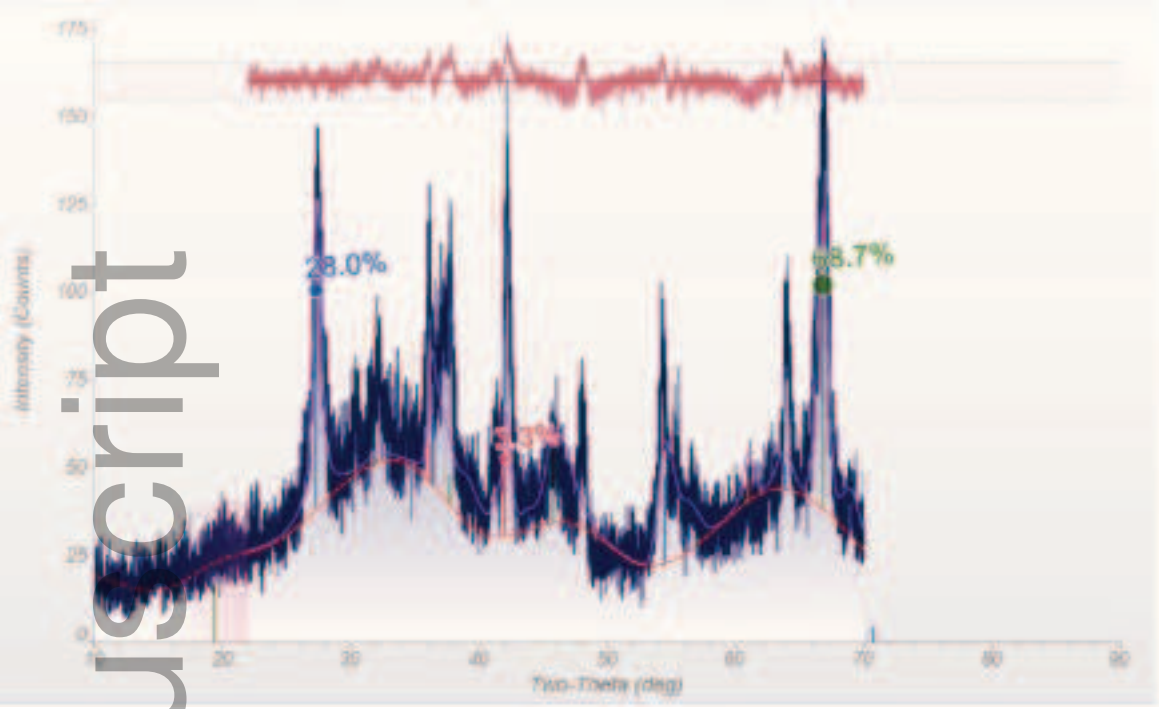

jace_15303_f3.tiff

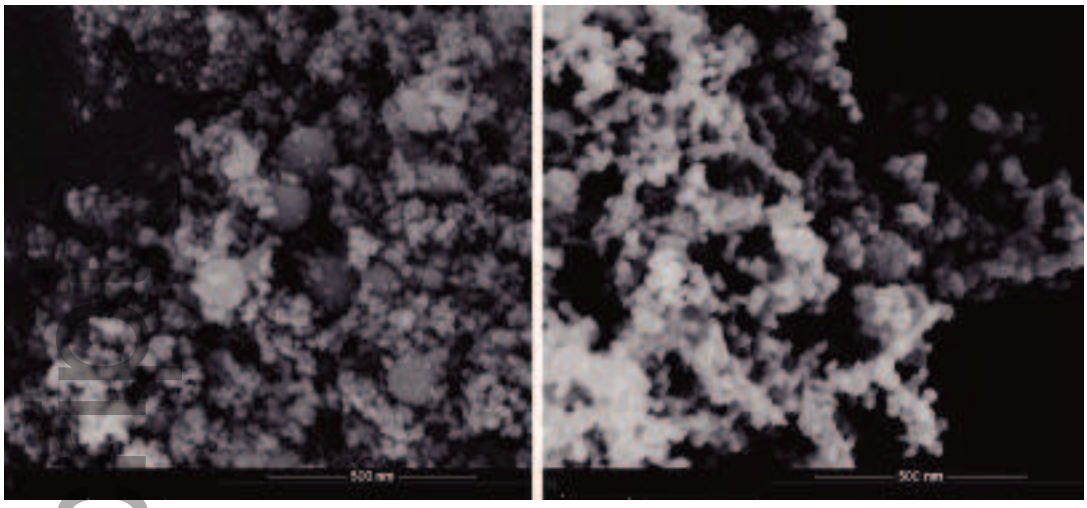

jace_15303_f4.tiff

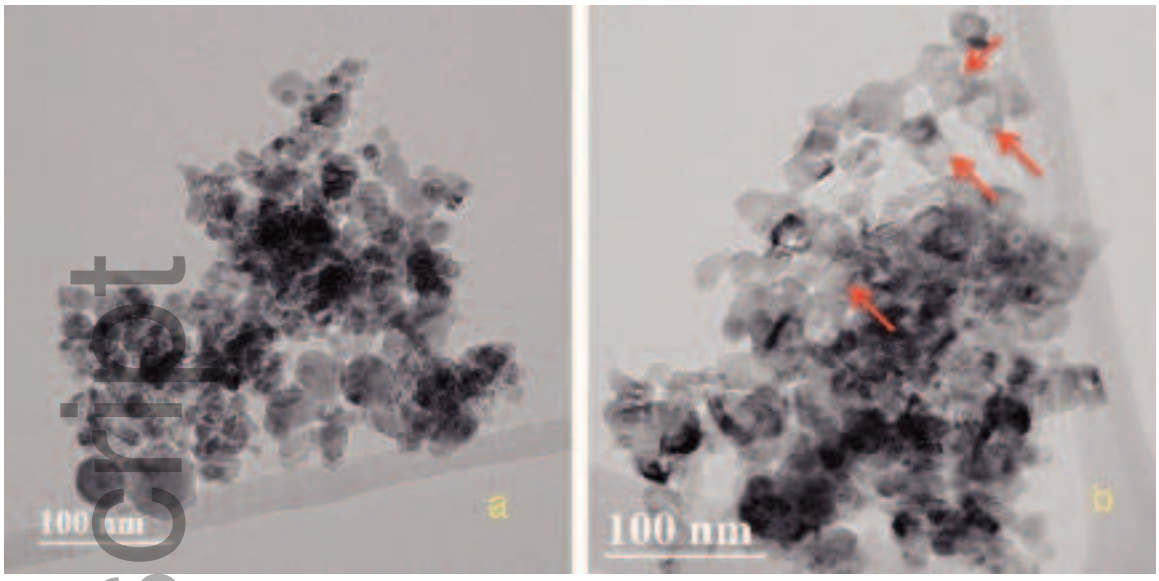

jace_15303_f5.tiff

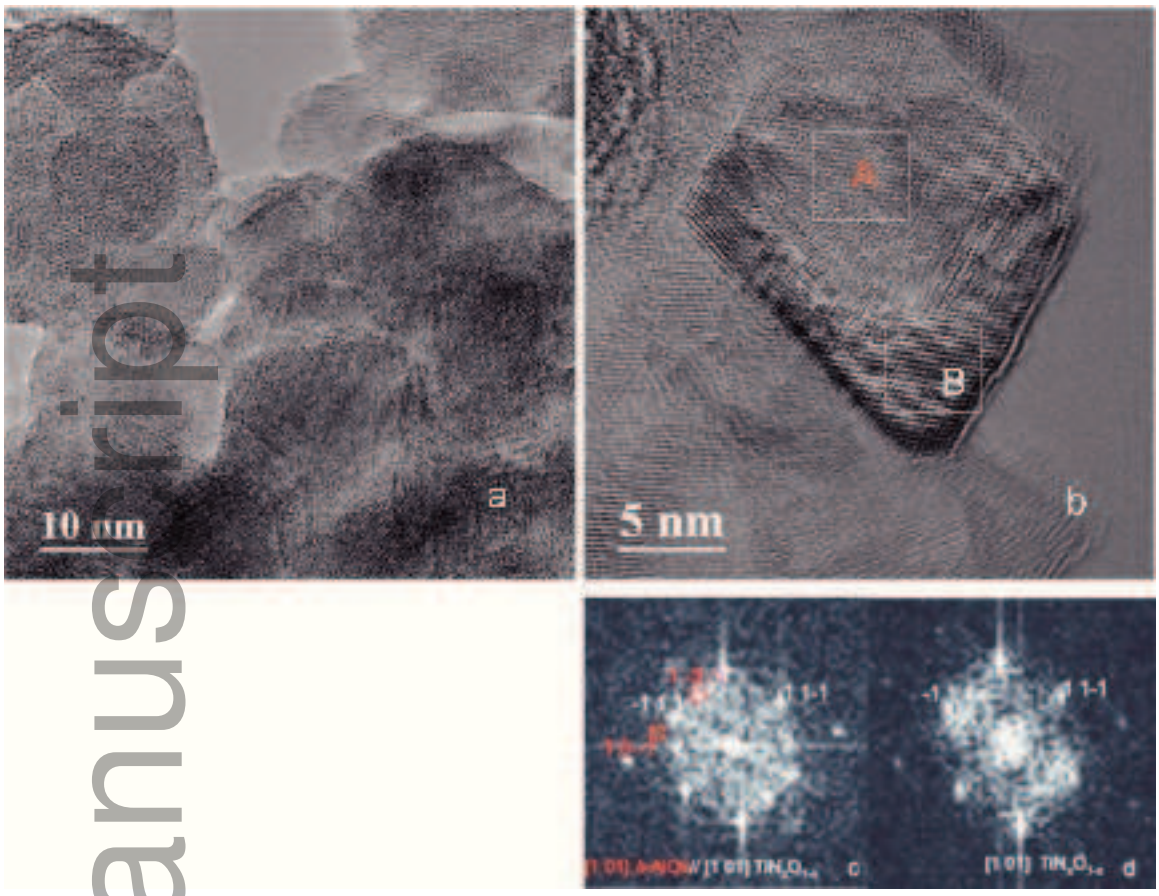

jace_15303_f6.tiff

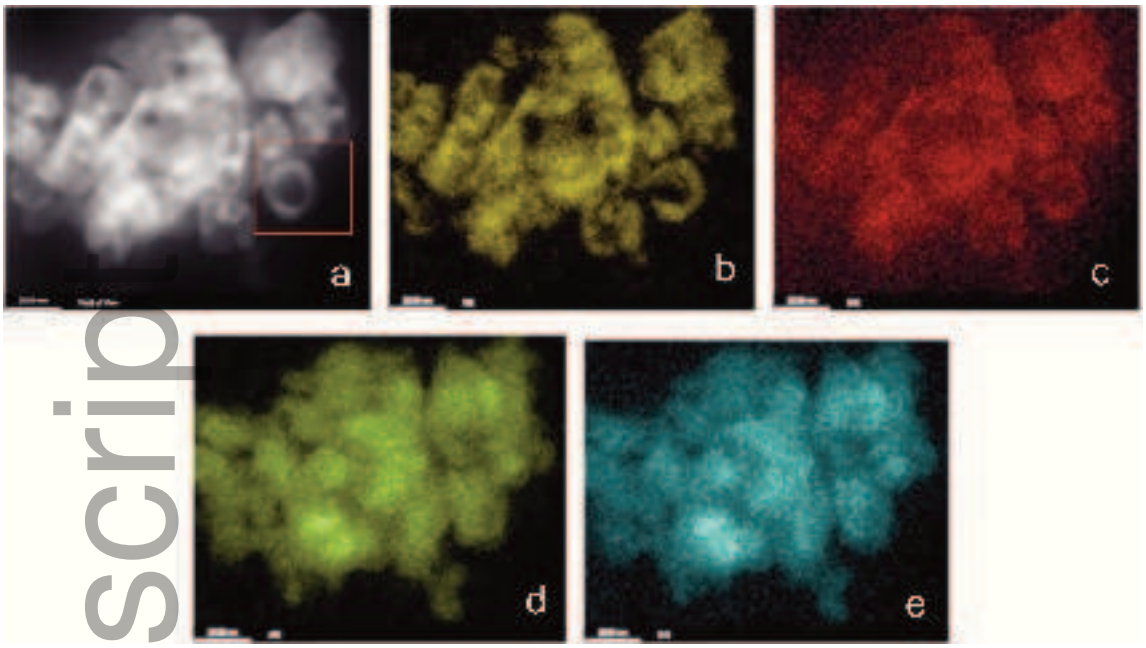

jace_15303_f7.tiff

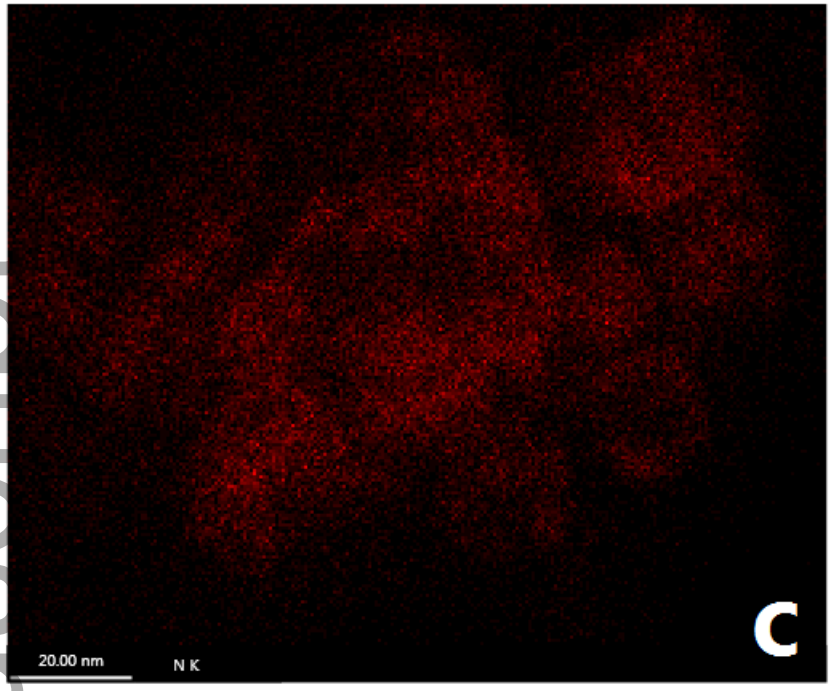

jace_15303_f7c.tif

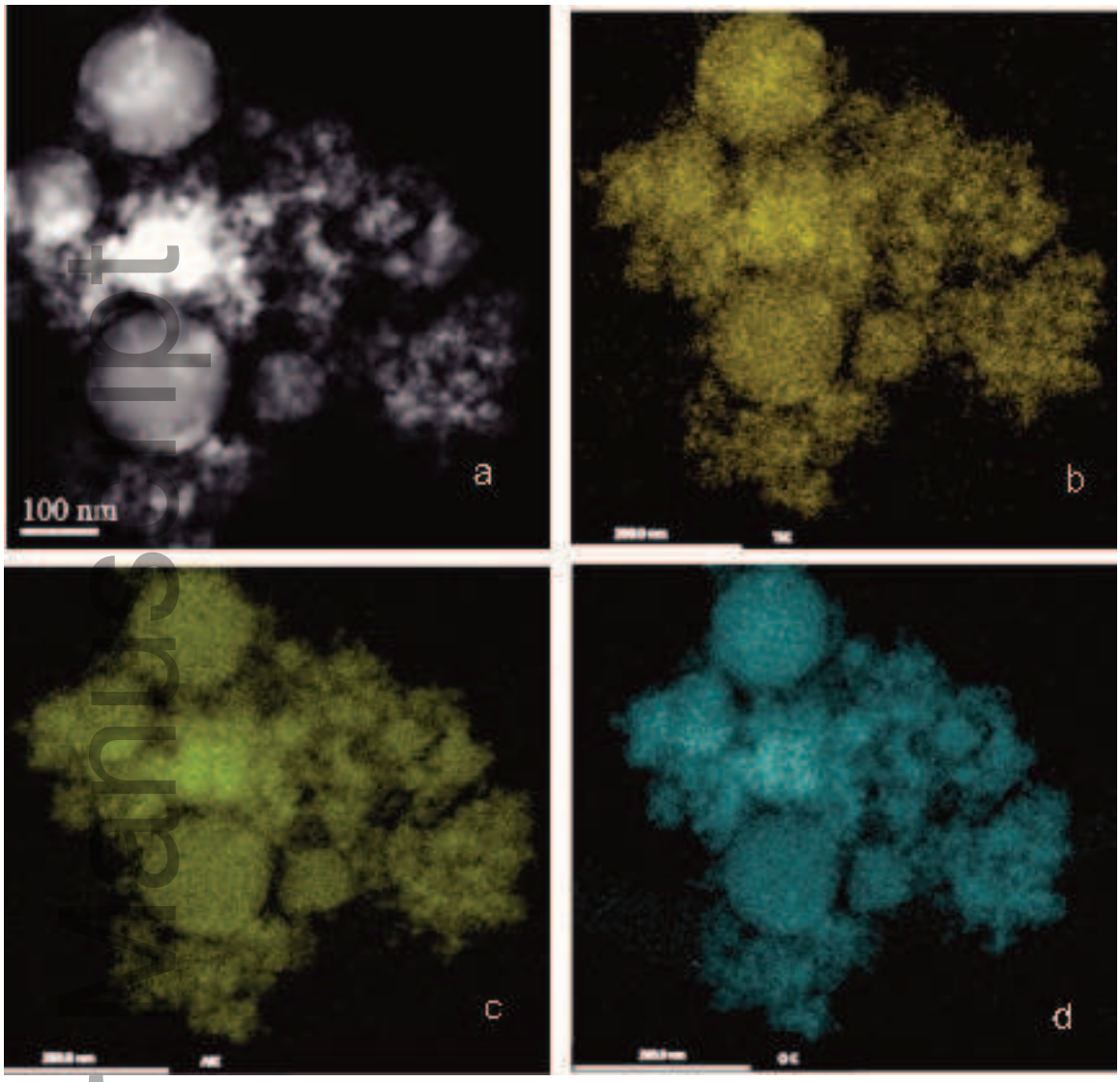

jace_15303_f8.tiff

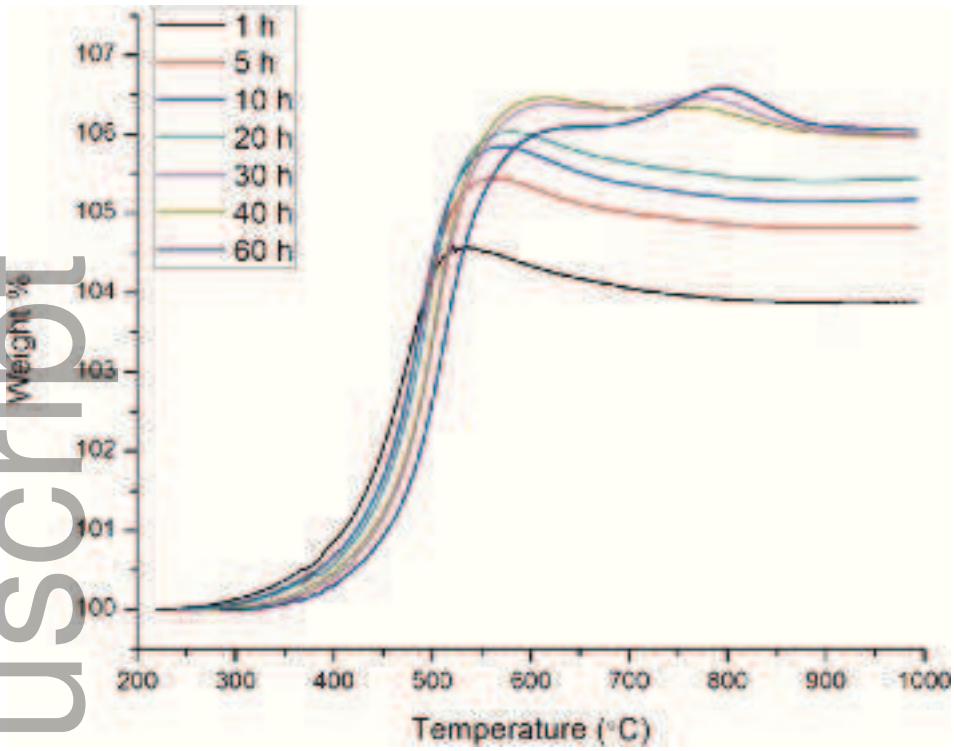

jace_15303_f9.tiff

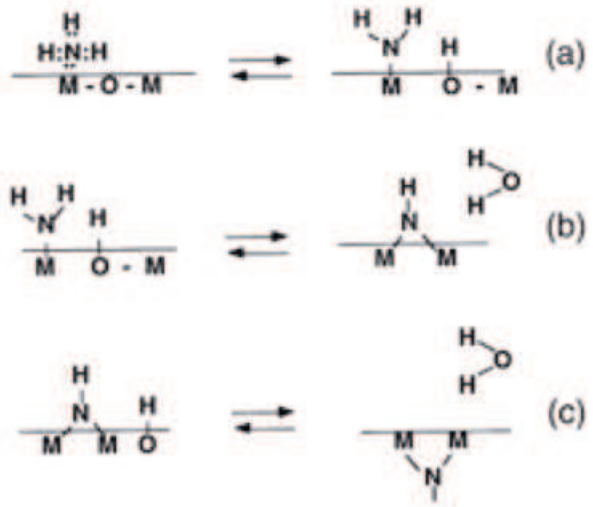

jace_15303_f10.tiff